GEOSCIENCE FRONTIERS 2(1) (2011) 17–22

available at www.sciencedirect.com

China University of Geosciences (Beijing)

GEOSCIENCE FRONTIERS

journal homepage: www.elsevier.com/locate/gsf

ORIGINAL ARTICLE

Anatomy of the 2009 Fiordland earthquake (M_w 7.8), South Island, New Zealand

P. Mahesh, Bhaskar Kundu*, J.K. Catherine, V.K. Gahalaut

National Geophysical Research Institute, Council of Scientific and Industrial Research, Hyderabad 500007, India

Received 20 November 2010; accepted 6 December 2010
Available online 5 January 2011

KEYWORDS
Fiordland subduction zone;
Global Positioning System;
Coulomb stress;
Alpine fault

Abstract We have analyzed the July 15, 2009, Fiordland earthquake (M_w 7.8), which occurred in the southwestern part of the South Island of New Zealand. This thrust-related earthquake in the southern Fiordland subduction zone is the largest New Zealand earthquake in the past 80 years. We have constrained a rupture model for this earthquake using coseismic offsets derived from the continuous geodetic network (Global Positioning System) of the New Zealand Institute of Geological and Nuclear Sciences (GNS Science). Our analysis concludes that this earthquake significantly increased the Coulomb stress on the overriding plate, particularly on the offshore portion of the Alpine fault.
© 2011, China University of Geosciences (Beijing) and Peking University. Production and hosting by Elsevier B.V. All rights reserved.

1. Introduction

The importance of Global Positioning System (GPS) measurements in constraining and characterizing earthquake rupture and understanding the mechanism of earthquakes has been widely recognized. GPS measurements have been particularly useful in the case of major and great earthquakes that cause large and far-field coseismic offsets. Here, we use GPS measurements to constrain the rupture of the July 15, 2009, southern New Zealand Fiordland earthquake and evaluate its implications for seismic hazard assessment. This thrust-related earthquake, the largest New Zealand earthquake in the past 80 years, occurred within the Fiordland subduction zone of southwestern South Island. The earthquake occurred at 9:22 UTC; its epicenter was in Dusky Sound about 155 km WNW from Invercargill and 182 km WSW from Queenstown. The M_w 7.8 earthquake ruptured the plate boundary interface between the subducting Australian plate and the overlying Pacific plate, with the deeper end of the rupture underlying the coast of Fiordland, a sparsely populated region in the southwestern part of the South Island. This event appears to be one of the better recorded shallow (ca. 12 km) subduction thrust earthquakes and could be evaluated because of the recent deployment of seismographs and a continuous GPS network in Fiordland as part of the GeoNet project run by GNS Science (http://www.geonet.org.nz).

* Corresponding author.
E-mail address: rilbhaskar@gmail.com (B. Kundu).
1674-9871 © 2011, China University of Geosciences (Beijing) and Peking University. Production and hosting by Elsevier B.V. All rights reserved.

Peer-review under responsibility of China University of Geosciences (Beijing).
doi:10.1016/j.gsf.2010.12.002

Production and hosting by Elsevier

2. Geodynamic setting

The North and South Islands of the New Zealand straddle the boundary between the Australian and Pacific plates. Along this boundary through the Fiordland region of southern New Zealand, the Australian and Pacific plates are converging very obliquely at the rate of about 34 mm per year (Fig. 1). In southwestern-most South Island, this motion is accommodated by oblique convergence at the Puysegur Trench. However, farther north along the South Island's west coast, the relative plate motion is accommodated by oblique strike-slip movement along the Alpine fault (Norris and Cooper, 2000) that drives uplift of the Southern Alps (Fig. 1; Adams and Ware, 1977; Adams, 1980; Allis, 1981; Davey and Smith, 1983). Northern Fiordland has been seismically very active since 1988, and has experienced a series of six large earthquakes of $M_w > 6$. However, southern Fiordland has been surprisingly quiet. The Fiordland M_w 7.8 earthquake broke this quiescence, with its magnitude comparable to that of the northern South Island Murchison earthquake of 1929 and the destructive North Island Hawke's Bay earthquake of 1931.

3. Geodetic data (GPS) analysis

To understand coseismic deformation in the South Island, we analyzed the GPS data from the continuous GPS network in Fiordland. We used data for the period 12th–18th July 2009, which include data three days prior to and three days after the earthquake. We processed GPS data from the sites BLUF, HAAS, LEXA, MAVL, and PYGR (Fig. 1) for that period, using GAMIT/GLOBK 10.35 software (Herring, 2005; King and Bock, 2005) to estimate time series of the station coordinates in ITRF05 reference frame. The loosely constrained solutions from our processing were combined with loosely constrained solutions of eight IGS stations namely CHAT, CNCL, DUND, KARA, MTJO, OUSD, QUAR and WAKA, the data which are the available from the Scripps Orbital and Positioning Analysis Centre (SOPAC; http://garnet.ucsd.edu). We were thus able to identify significant offsets in GPS time series due to the earthquake (Figs. 1 and 2; Table 1). The earthquake caused permanent westward coseismic displacements of about 1.7 cm at Alexandra (LEXA), 2.6 cm at Haast (HAAS), 2.8 cm at Bluff (BLUF), 5.5 cm at Mavora Lakes (MAVL) and 30 cm at Puysegur Point (PYGR). Significant postseismic deformation can also be seen at PYGR (Fig. 2).

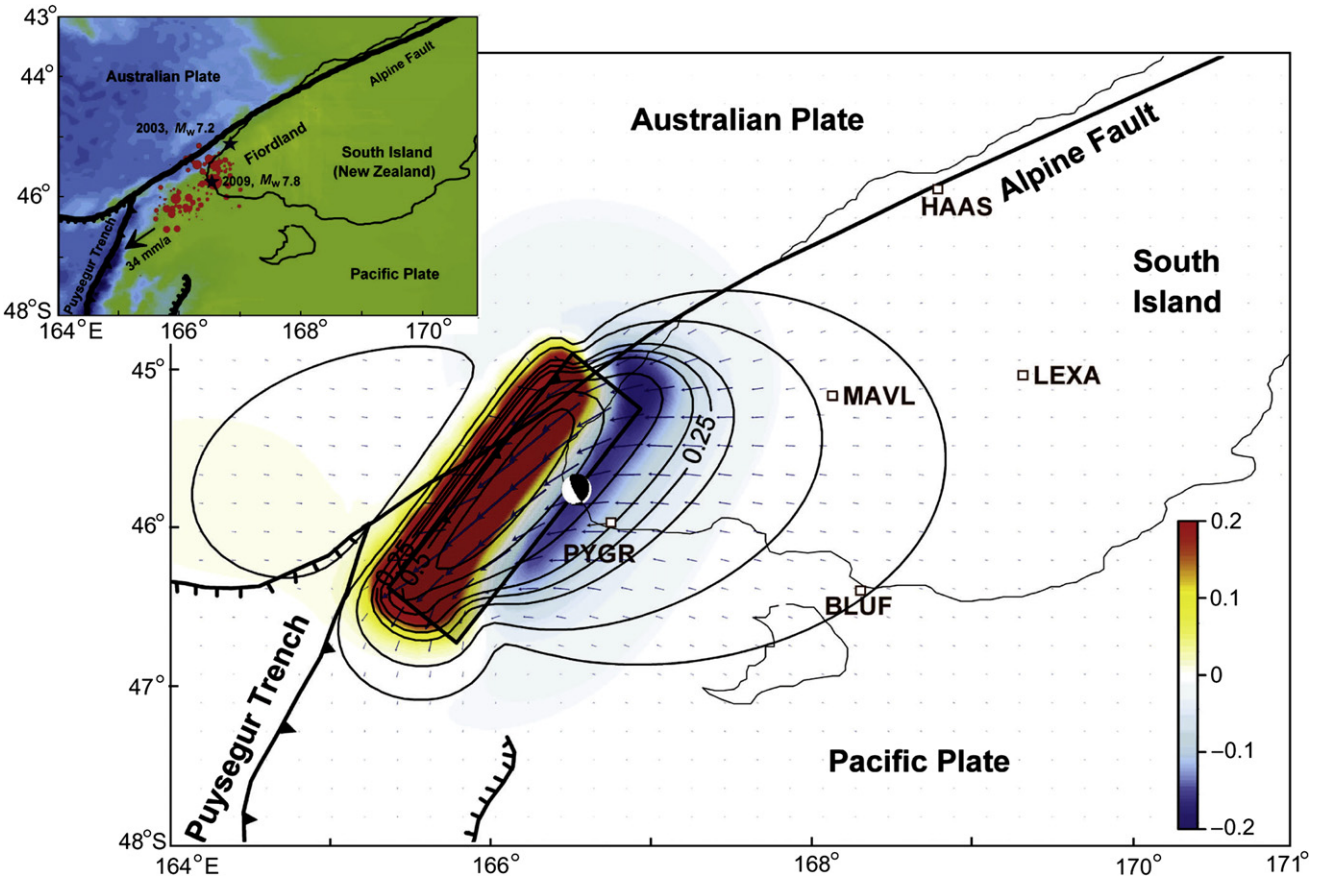

Figure 1 Bathymetry, general tectonics, earthquakes and rupture in the South Island (New Zealand). The main shock of the 15 July 2009 Fiordland New Zealand earthquake epicenter along with its aftershocks are shown by star and filled red circles in the inset. Main figure shows simulated horizontal (arrows and contours) and vertical (superimposed colour image) coseismic displacement (in meter) due to slip on the south-east dipping fault plane of the 2009 South Island earthquake. Locations of the continuous GPS sites (PYGR, BLUF, MAVL, LEXA and HAAS) and the estimated coseismic offsets from GPS measurements are also shown. Rectangle shows the surface projection of the south-east dipping rupture. Note the non-uniform contour interval.

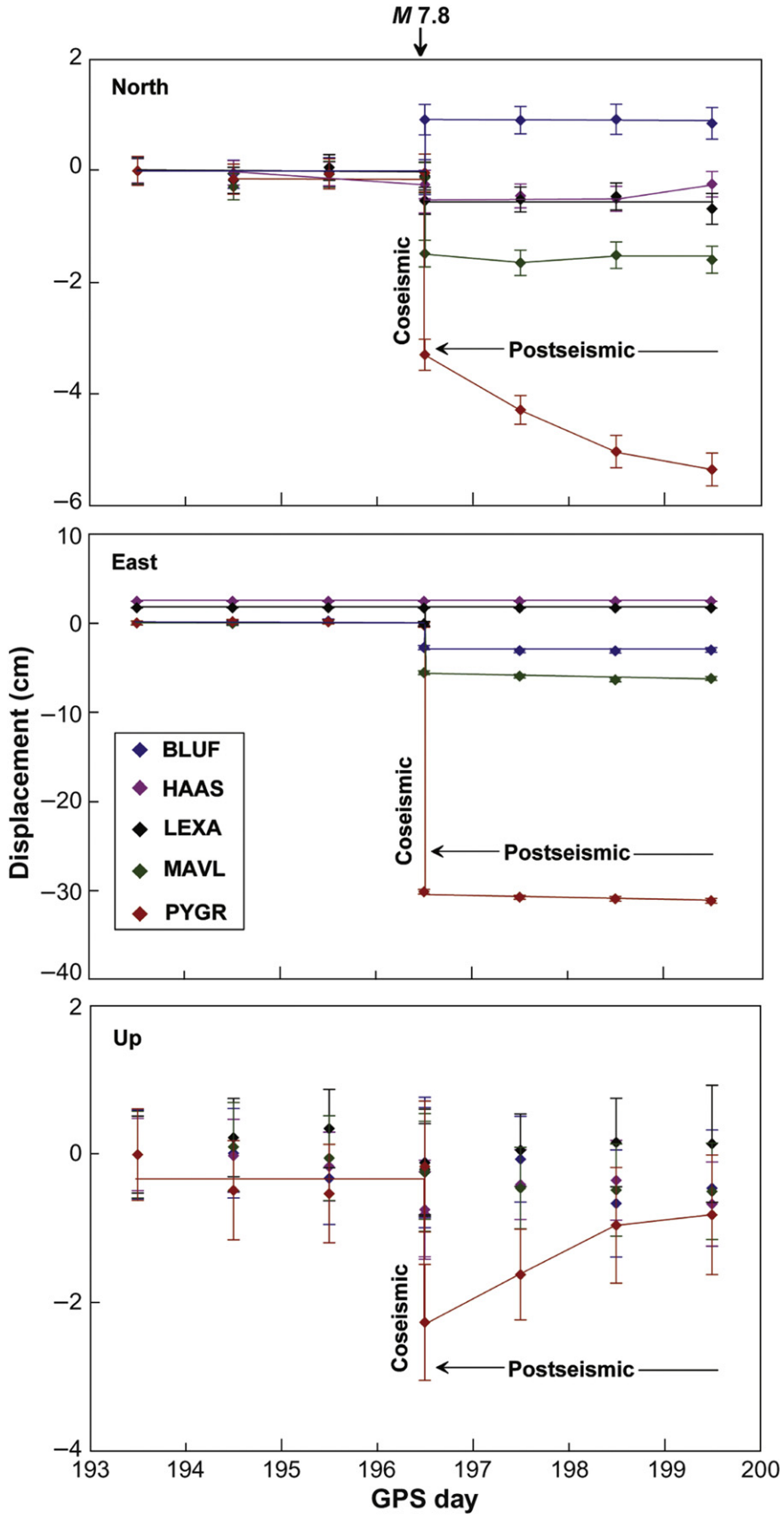

Figure 2 Temporal variation of horizontal displacement in the north, east and vertical directions at continuous GPS sites at BLUF, HAAS, LEXA, MAVL and PYGR. Coseismic offset at all the sites can be noted by the jump. The PYGR site shows maximum coseismic offset and postseismic displacement in the north and up component.

Table 1 Coseismic offsets at continuous GPS sites and simulated displacement due to slip on rupture.

Site name	Coseismic offset (cm)			Simulated displacement due to slip on rupture (cm)		
	North	East	Vertical	North	East	Vertical
BLUF	1.0	−2.7	–	0.9	−2.4	–
HAAS	−0.3	2.6	–	−0.2	3.6	–
LEXA	−0.5	1.8	–	−0.4	2.4	–
MAVL	−1.5	−5.5	–	−2.1	−4.8	–
PYGR	−3.0	−30.1	−2.0	−2.9	−31.7	−1.8

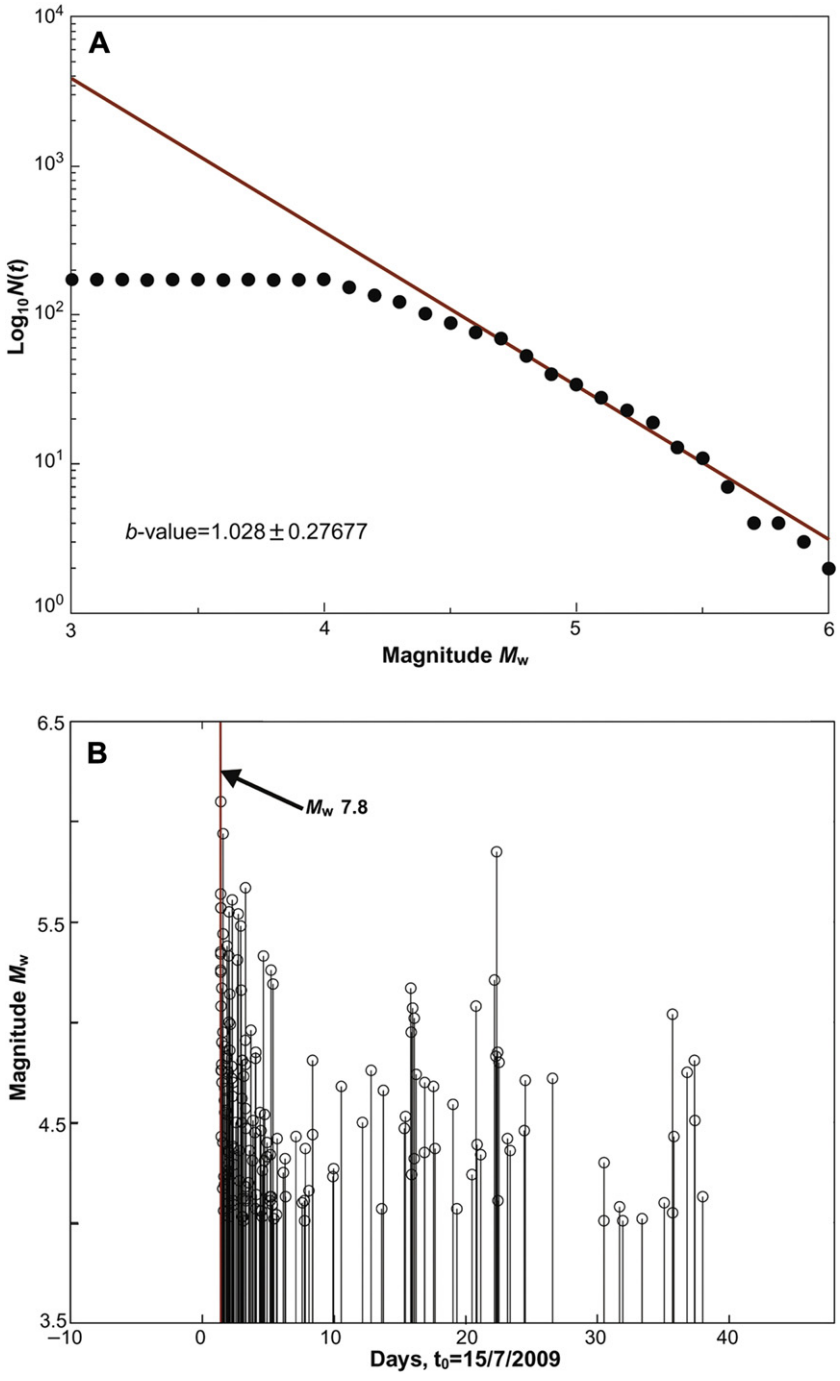

Figure 3 Gutenberg-Richter law (3A) and temporal distribution of aftershocks (3B). Note the *b* value indicates a typical subduction zone event.

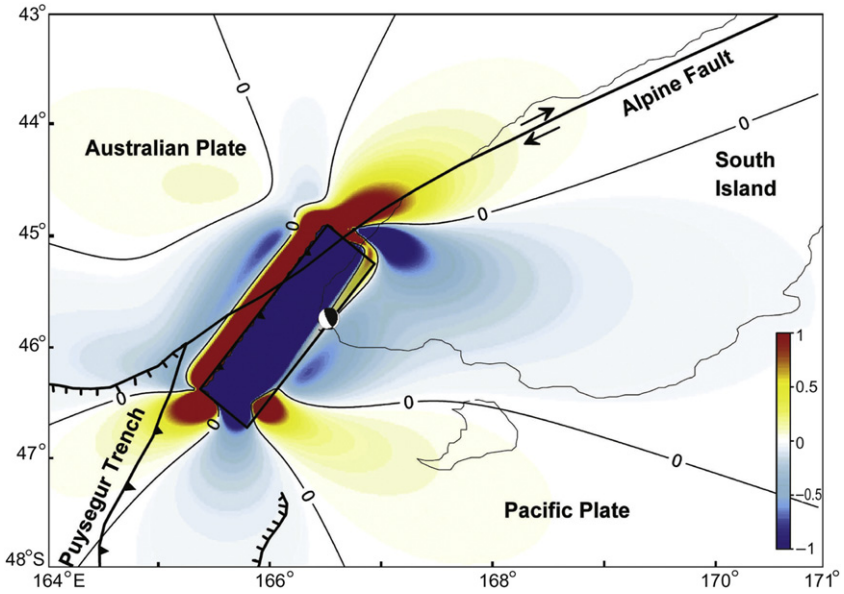

Figure 4 Change in the Coulomb failure stress (ΔCFS) in bar, due to slip on the rupture (with strike dip and rake as 26°, 24°, and 140°, respectively), resolved on the dextral strike-slip Alpine fault. Hot colors encourage failure while cool colors discourage failure. Note the increase in ΔCFS on Alpine fault.

4. Rupture model using the coseismic offsets

The fault plane solution for this earthquake indicates low-angle thrust faulting on a plane which has the same strike and dip as those of the shallow part of the plate interface. The aftershock zone clearly abuts that of the 2003 M_w 7.2 subduction thrust earthquake in northern Fiordland (Fig. 1). We estimated a 2009 rupture length and width of 125 and 38.6 km, respectively, from the earthquake magnitude using scaling relations (Wells and Coppersmith, 1994) and from the extent of the aftershock zone. The aftershocks are located at the two ends of the rupture zone and are mainly a mixture of reverse faulting and strike-slip faulting mechanisms reflecting the complex tectonics of the region. A notable feature of this earthquake is the relatively small amount of radiated seismic energy, which corresponds to an energy magnitude (M_e) of only 7.5. This fact combined with the seaward direction of the rupture, can help explain the low level of damage resulting from the earthquake. We used Okada's (1992) formulation to estimate the coseismic displacement due to uniform slip of 2 m on a rectangular rupture area in elastic half space. The updip and downdip edges of the rupture are estimated as 10 and 25.7 km, respectively. The simulated displacement at the continuous GPS sites PYGR, MAVL, BLUF, LEXA and HAAS due to fault plane slip (with strike dip and rake as 26°, 24°, 140°) is consistent with the offsets derived from the GPS observations (Fig. 1, Table 1). A moment magnitude is estimated as 7.6 by using the derived rupture parameters. Because all the sites are located on one side of the fault, i.e. on the hanging wall, we did not attempt estimating non-uniform slip over a rupture of arbitrary shape and, thus, preferred a simple rectangular model with uniform slip. Because of this limitation, a small portion of rupture (the northern updip edge) appears to cut across the fault, which may not be the case in reality.

5. The *b* value estimation

There is a duality between space and time window in *b* value estimations. If a complete description of the Gutenberg–Richter (GR) law (Gutenberg and Richter, 1949) is expected (i.e., there is a linear part of this law), one must consider a small region over a longer time window (t) of observation, or a greater region over a smaller time window (Legrand et al., 2004). Hence, spatial and temporal windows cannot be chosen independently. Once the spatial window is taken, the temporal window should be longer enough that all magnitude ranges are sampled during this time window. If the spatial widow is divided into small cells, it is not certain that each cell will have the same number of events. Thus, the GR law may not be the equally representative in space and may not be applied in cells with few data sets. At the same time, local seismic networks with good azimuthally covered station locations also enhance the precision of the GR law. Keeping this in mind, we have taken epicenter locations (Fig. 1) of the Fiordland earthquake (M_w 7.8) and its aftershocks from the GeoNet project run by GNS Science (http://www.geonet.org.nz). The *b* value of the GR law was calculated with the maximum likelihood method and for the case of single slope we generally use the famous method of Aki (1965). The Fiordland earthquake and its aftershock sequence are typically characterized by a GR law with single *b* value: 1.028 ± 0.27677 (Fig. 3). Thus it clearly indicates a tectonic scenario (i.e., typical subduction zone event).

6. Seismic hazard assessment

The most interesting aspect of this earthquake is radiation of small amount of seismic energy and its slow release. This probably explains why the damage was less than that expected for this size of the earthquake. A few single-story structures overlying the rupture zone suffered no structural damage. It is also reported that the incidence of landslides in the steep-sided fiords was significantly less than that due to the smaller 2003 M_w 7.2 earthquake (Fig. 1). Because the rupture zone of the 2009 earthquake is located mostly beneath the land and continental slope, it could only generate a local tsunami. The largest observed tsunami wave was about 1 m at the tide gauge of Jackson Bay, near Haast (Fig. 1), some 250 km northeast of the rupture zone.

We calculated Coulomb failure stress (ΔCFS) (King et al., 1994; Toda and Stein, 2002; Lin and Stein, 2004) due to slip on the south-east dipping plane. We assumed a coefficient of friction as 0.65. Our computations suggest that the ΔCFS increased on faults in the overlying plate, particularly on the offshore portion of the Alpine fault (Fig. 4). This significant increase in the Coulomb stress indicates that the occurrence of this subduction zone thrust earthquake has brought the Alpine fault closer to the failure.

7. Conclusions

Our study leads to the following salient conclusions:

(1) The 2009 New Zealand Fiordland earthquake (M_w 7.8) occurred in a South Island region of dense GPS and seismic network as part of the GeoNet project run by GNS Science. Thus, the constraints from GPS-derived coseismic offsets characterizing earthquake rupture, the ongoing postseismic deformation scenario, and an understanding of earthquake occurrence process in the Fiordland region are clearly highlighted in our present study.

(2) We further identify that this earthquake significantly increased the Coulomb stress (ΔCFS) on the overriding plate, particularly on the offshore portion of the Alpine fault. This is relevant regarding future seismic hazard assessment of the Fiordland region.

Acknowledgement

We thank the Council of Scientific and Industrial Research (CSIR) and Ministry of Earth Sciences (MoES), New Delhi for financial support.

References

Adams, J., 1980. Contemporary Uplift and Erosion of the Southern Alps. Geological Society of America Bulletin, Part II, New Zealand, 91; pp. 1–114.

Adams, R.D., Ware, D.E., 1977. Subcrustal earthquakes beneath New Zealand, location determined with a laterally inhomogeneous model. New Zealand Journal of Geology and Geophysics 20, 59–83.

Aki, K., 1965. Maximum Likelihood Estimate of B in the Formula LogN = a − BM and Its Confidence Limits. Bulletin of Earthquake Research Institute. The University of Tokyo, 43, pp. 237–239.

Allis, R.G., 1981. Continental underthrusting beneath the southern Alps of New Zelanan. Geology 9, 303–307.

Davey, F.J., Smith, E.G.C., 1983. The tectonic setting of the Fiordland region, south-west New Zealand. Geophysical Journal Royal Astronomical Society 72, 23–38.

Gutenberg, B., Richter, C., 1949. Seismicity of the Earth and Associated Phenomena. Princeton University Press, Princeton, New Jersey.

Herring, T.A., 2005. GLOBK, Global Kalman Filter VLBI and GPS Analysis Program, Version 10.2, Report. Department of Earth, Atmospheric and Planetary Sciences, Massachussetts Institute of Technology.

King, G.C.P., Stein, R.S., Lin, J., 1994. Static stress changes and the triggering of earthquakes. Bulletin of the Seismological Society of America 84 (3), 935–953.

King, R.W., Bock, Y., 2005. Documentation for the GAMIT GPS Analysis Software, Release 10.2, Report. Department of Earth, Atmospheric and Planetary Sciences, Massachussetts Institute of Technology.

Legrand, D., Villagómez, D., Yepes, H., Calahorrano, A., 2004. Multifractal dimension and *b* value analysis of the 1998-1999 Quito swarm related to Guagua Pichincha volcano activity, Ecuador. Journal of Geophysical Research 109 (B0137) doi: 10.1029/2003JB002572.

Lin, J., Stein, R.S., 2004. Stress triggering in thrust and subduction earthquakes, and stress interaction between the southern San Andreas and nearby thrust and strike-slip faults. Journal of Geophysical Research 109 (B02303) doi: 10.1029/2003JB002607.

Norris, R.J., Cooper, A.F., 2000. Late Quaternary slip rates and slip partitioning on the Alpine fault, New Zealand. Journal of Structural Geology 23, 507–520.

Okada, Y., 1992. Internal deformation due to shear and tensile faults in a half-space. Bulletin of the Seismological Society of America 82 (2), 1018–1040.

Toda, S., Stein, R.S., 2002. Response of San Andreas fault to the 1983 Coalinga Nunez earthquakes: an application of interaction-based probabilities for Parkfield. Journal of Geophysical Research 107 (B6) doi: 10.1029/2001JB000172.

Wells, D.L., Coppersmith, K.J., 1994. New empirical relationships among magnitude, rupture length, rupture width, rupture area, and surface displacement. Bulletin of the Seismological Society of America 84, 975–1002.